Surfactant Templated Assembly of Cubic Mesostructured Semiconductors Based on $[Sn_2Se_6]^{4-}$ and Pt^{2+} in Single-Crystal Form.

Pantelis N. Trikalitis and Mercouri G. Kanatzidis
Department of Chemistry, Michigan State University, East Lansing, MI 48824

Abstract

Mesostructured non-oxidic materials with cubic *Ia*-3*d* symmetry were prepared by linking $[Sn_2Se_6]^{4-}$ clusters with Pt^{2+} in the presence of surfactant molecules. The use of long chain pyridinium-based surfactants (octadecyl- and eicosadecyl) afforded materials with exceptionally high cubic pore order and single-crystal particle morphology. By contrast trimethylammonium-based surfactants produced cubic mesostructured solids with inferior overall quality. We have also synthesized materials with significantly lower surfactant content by increasing the Pt^{2+}:$[Sn_2Se_6]^{4-}$ molar ratio, while maintaining the cubic pore symmetry. All materials are semiconductors with energy band-gap in the range $0.9<E_g<1.8$ eV.

Introduction

Since the first report of mesoporous silicates a decade ago, numerous mesoporous and mesostructured silica-based materials, metals oxides and pure metals have been reported and significant advances were made in controlling the overall symmetry.[1] A unique feature in these materials is periodic long-range pore order either in two- or three-dimensions. Among them the cubic three-dimensional (3D) pore structures are recognized to be much more interesting in terms of their potential.[2] The vast majority of reports have focused on oxidic materials. However, three-dimensional periodically arranged pores in a non-oxidic semiconducting solid could modify the optoelectronic properties in way that has no precedent in bulk semiconductor analogues. Recently we reported for the first time the synthesis of non-oxidic cubic semiconducting materials in the form of single crystals using $[Sn_2Se_6]^{4-}$ anions (see scheme 1) as the chalcogenido building blocks and Pt^{2+} as the linkage metal, in the presence of octadecyl- or eicosadecylpyridinium molecules acting as the surfactant template.[3] Both inorganic building blocks present local square planar connectivity preference and as such define the only currently available system that leads to cubic chalcogenido mesostructures.[4] In this work we explored the role of the nature of the surfactant molecules in the assembly process as well as the possibility of synthesizing well-ordered cubic materials with low

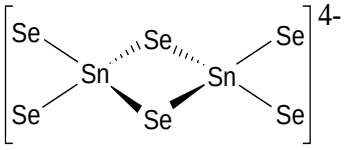

Scheme 1. Chalcogenido $[Sn_2Se_6]^{4-}$ building block.

surfactant content and presumably thicker inorganic walls using high Pt^{2+}:$[Sn_2Se_6]^{4-}$ molar ratios. We found that long chain (octadecyl- or eicosadecyl-) trimethylammonium-based surfactants also produced materials with cubic pore symmetry, however powder X-ray diffraction and scanning electron microscopy (SEM) images suggest, the overall quality is inferior as compared to the materials obtained with pyridinium-based surfactants. We succeeded also in synthesizing solids with well-ordered cubic pore structure, containing less than a half amount of surfactant compared to the original materials. These new materials are expected to be more robust in attempts to remove the surfactant and access the pore space.

Experimental

The synthesis of cubic materials with single crystal particle morphology denoted as *c*-C_nPyPtSnSe (n=18, 20) have been published in detail elsewhere.[3] The corresponding trimethylammonium-based cubic materials denoted as *c*-C_nTMAPtSnSe (n=18, 20) were synthesized by a similar procedure. Mesostructured materials with higher platinum content were synthesized utilizing C_{20}PyBr surfactant molecules and 2:1 and 3:1 Pt^2:$[Sn_2Se_6]^{4-}$ molar ratio and denoted as *c*-C_{20}PyPt2SnSe and *c*-C_{20}PyPt3SnSe respectively. In all cases formamide (FM) used as a solvent and syntheses were performed in a glove box under nitrogen.

Results And Discussion

The elemental composition of the mesostrucutred platinum tin selenides was determined by energy-despersive microprobe analysis (SEM/EDS), elemental C, H, N and thermogravimetric analysis (TGA), see Table 1. In all cases the Pt:Sn ratio was found to be very close to the value expected from the synthesis suggesting the quantitative incorporation of platinum into the inorganic framework. Moreover it is important to note the significant lower surfactant content in the solids with high Pt:Sn ratio. For *c*-C_nPyPtSnSe materials the results are consistent with the stoichiometric formula $(C_nPy)_2Pt[Sn_2Se_6]$ (n=18, 20). However for *c*-C_{20}PyPt2SnSe and *c*-C_{20}PyPt3SnSe solids the data suggest a more complex charge balancing formula presumably containing more

Table 1. Summary of elemental analysis and colors for the cubic mesostructured platinum tin selenides.

Sample	% C, H, N	Pt:Sn:Se	Color
c-C_{18}PyPtSnSe	32.92, 5.16, 1.93	0.96:2:5.8	Dark-brown
c-C_{20}PyPtSnSe	36.14, 5.61, 1.78	1.03:2:5.8	Dark-brown
c-C_{18}TMAPtSnSe	29.71, 5.65, 1.87	0.9:2:5.3	Black
c-C_{20}TMAPtSnSe	32.95, 5.90, 1.94	0.9:2:5.4	Black
c-C_{20}PyPt2SnSe	23.02, 3.32, 1.30	2.1:2:2:5.9	Black
c-C_{20}PyPt3SnSe	15.64, 2.29, 1.09	2.9:2:5.6	Black

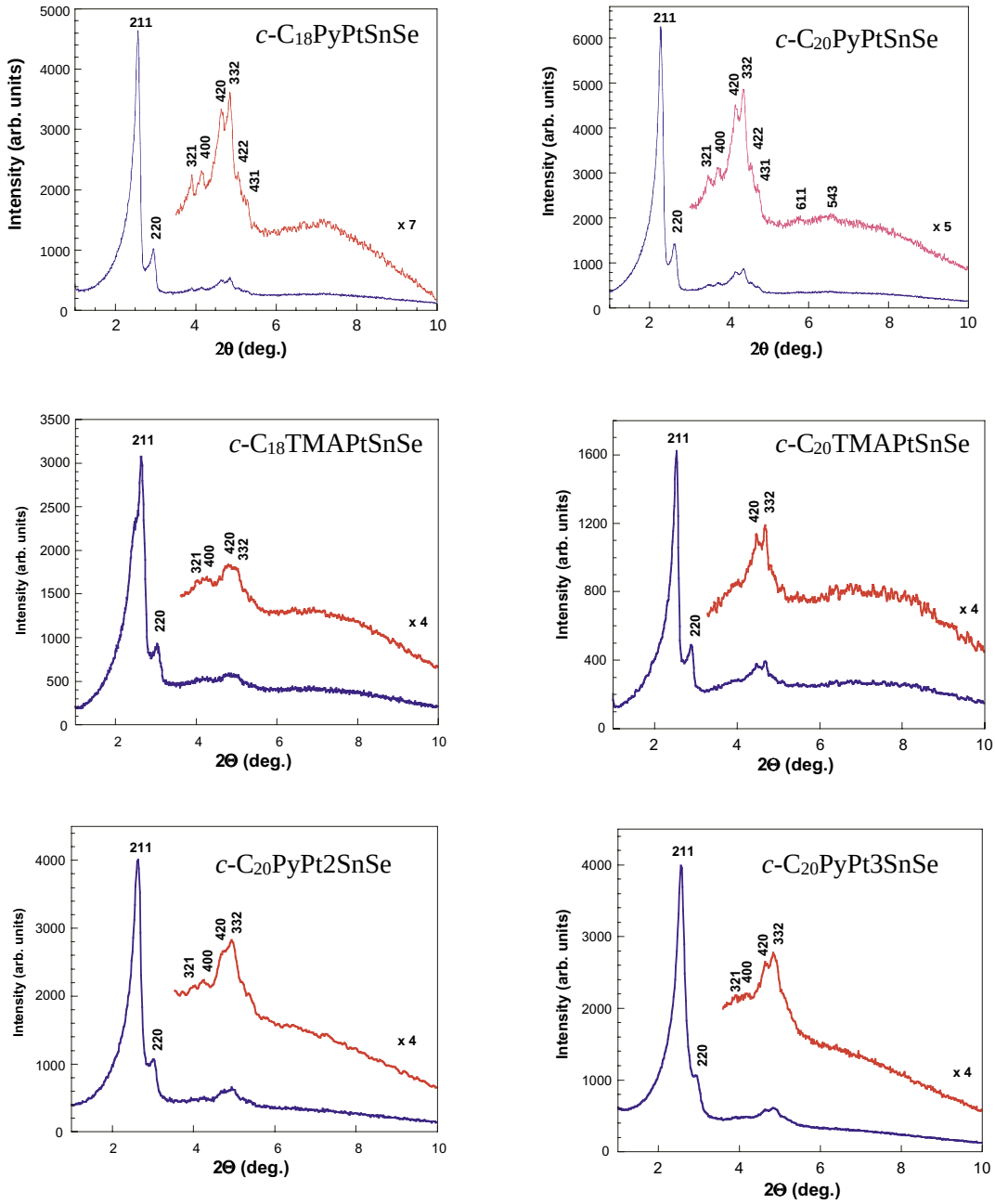

Figure 1 . X-ray powder diffraction patterns of mesostructured platinum tin selenides (CuKα radiation).

than one chalcogenido building blocks.

Shown in Figure 1 are the X-ray powder diffraction (XRD) patterns of the mesostructured platinium tin selenides. These patterns show up to 10 Bragg diffraction peaks in the low-angle $2^o < 2\theta < 7^o$ region resembling those of mesostructured cubic MCM-48 silica and accordingly are fully indexed to a cubic unit cell belonging to the

Ia-3*d* space group. A comparison of the XRD patterns between the *c*-C_nPyPtSnSe and *c*-C_nTMAPtSnSe (n=18, 20) materials reveal that the former show more and better resolved Bragg reflections suggesting a higher pore structural coherence. In other words although the pyridinium-based surfactants are not necessary in achieving the cubic pore symmetry however, they are important for synthesizing high-quality materials in terms of pore order with best single-crystal particle morphology. Based on XRD patterns and scanning electron microscopy images (SEM) (see below) there is no apparent difference in quality between the *c*-C_nPyPtSnSe materials as a function of the surfactant chain length, where in the case of *c*-C_{18}TMAPtSnSe and *c*-C_{20}TMAPtSnSe the latter shows improved cubic pore structure. It is significant that it is possible to synthesize materials with significant lower surfactant content while maintaining the cubic pore symmetry. These materials are well ordered (see XRD patterns in Figure 1) and have >50% lower surfactant content than the original material (see Table 1). This implies that may have a thicker inorganic wall structure that the *c*-C_nPyPtSnSe materials.

SEM images of *c*-C_nPyPtSnSe reveal that the particles are in the form of faceted single crystal with rhombic dodecahedral morphology as large as 2μm. Shown in Figure 2 are representative images of *c*-C_{20}PyPtSnSe cubosomes. The particles of *c*-C_{18}TMAPtSnSe product show highly irregular shape and size whereas those of *c*-C_{20}TMAPtSnSe appeared well faceted. These results suggest that under the present experimental conditions in contrast with the pyridinium-based materials, the surfactant chain length in the trimethylammonium-based solids plays a more important role in controlling the overall quality of the final product.

The cubic mesoscopic order confirmed with direct imaging by transmission electron microscopy (TEM). Figure 3 shows representative TEM images of *c*-C_{20}PyPtSnSe and *c*-C_{20}PyPt3SnSe materials where a remarkably uniform and extensive pore order is clearly visible. The estimated pore-pore separation and cell dimensions are in good agreement with those determined by XRD.

The thermal stability of the mesostructured solids was investigated with thermogravimetric analysis (TGA). Shown in Figure 4a are characteristic TGA curves of *c*-C_nPyPtSnSe, *c*-C_{20}PyPt2SnSe and *c*-C_{20}PyPt3SnSe. The compounds show no appreciable weight loss up to 150 ^{o}C. Between 150 ^{o}C and 450 ^{o}C weight loss occurs due to surfactant decomposition and the results are consistent with elemental C, H, N analysis. Note that *c*-C_{20}PyPt3SnSe show ~20% weight loss while *c*-C_{20}PyPtSnSe show ~45%. At 600 ^{o}C the inorganic residue is mainly crystalline PtSnSe as detected by powder X-ray diffraction.

The optical absorption properties of the materials were investigated with solid-state diffuse reflectance UV-vis/near-IR spectroscopy. All solids posses well-defined absorptions associated with band gap transition in the energy range 0.9-1.8 eV, see Figure 4b.

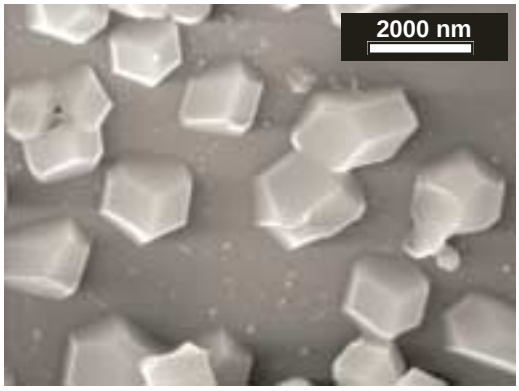

c-C_{20}PyPtSnSe

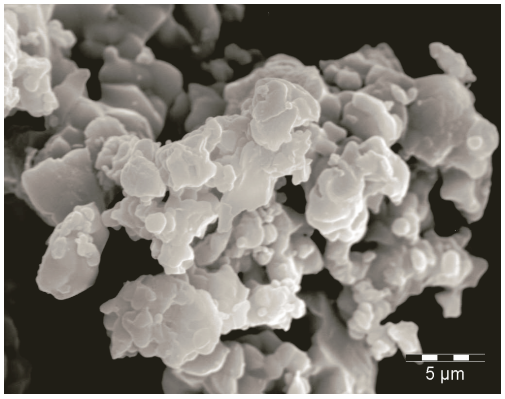

c-C_{18}TMAPtSnSe

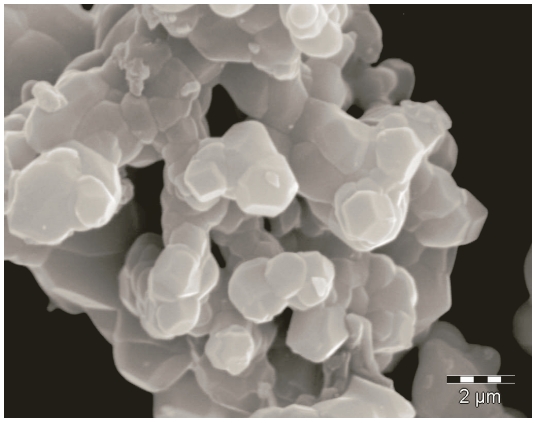

c-C_{20}TMAPtSnSe

Figure 2. Scanning electron microscopy images of cubic mesostructured platinum tin selenides.

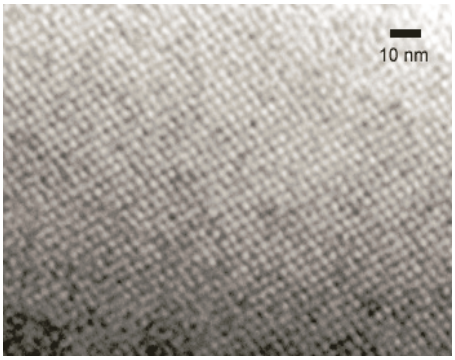

c-C_{20}PyPtSnSe particle viewed down the [110] cubic plane.

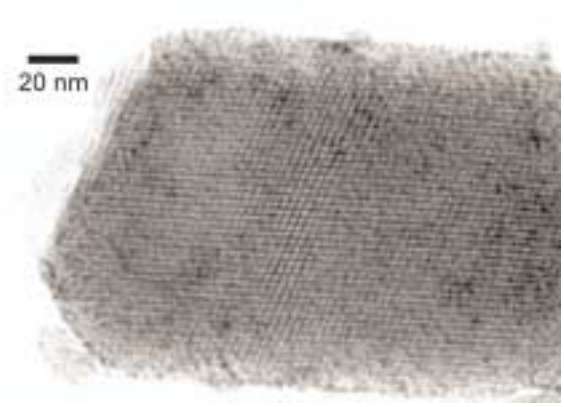

c-C_{20}PyPt3SnSe particle viewed down the [110] cubic plane.

Figure 3. Transmission electron microscopy images of cubic mesostructured platinum tin selenides.

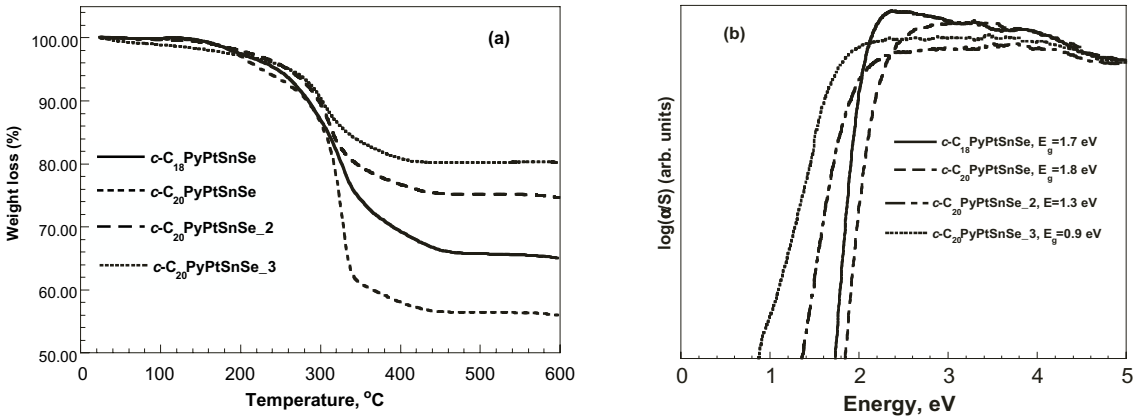

Figure 4. (a) TGA curves of *c*-C_nPyPtSnSe, *c*-C_{20}PyPt2SnSe and *c*-C_{20}PyPt3SnSe under nitrogen flow. (b) Solid-state UV-vis absorption spectra of *c*-C_nPyPtSnSe, *c*-C_{20}PyPt2SnSe and *c*-C_{20}PyPt3SnSe.

The band gap narrows in going from *c*-C_nPyPtSnSe to *c*-C_{20}PyPt2SnSe and *c*-C_{20}PyPt3SnSe materials. These differences are attributed to the different chemical composition of the inorganic framework between these materials.

Conclusions

The assembly of Pt^{2+} and $[Sn_2Se_6]^{4-}$ in the presence of various surfactant molecules lead to a new class of mesostructured materials with cubic *Ia*-3*d* symmetry and single-crystal particle morphology. The inorganic framework composition can considerably be varied while maintaining the cubic symmetry and pore order. The present results underscore the critical role certain well-selected chalcogenido building blocks can play in the construction of cubic 3D mesostructured semiconductors.

Acknowledgements

The support of this research by NSF-CRG Grant CHE 0211029 is gratefully acknowledged. This work made use of the SEM and TEM facilities of the Center of Advanced Microscopy at MSU.

References

(1) Davis, M. E. *Nature* **2002**, *417*, 813-821.

(2) Sakamoto, Y. H.; Kaneda, M.; Terasaki, O.; Zhao, D. Y.; Kim, J. M.; Stucky, G.; Shim, H. J.; Ryoo, *Nature* **2000**, *408*, 449-453.

(3) Trikalitis, P. N.; Rangan, K. K.; Bakas, T.; Kanatzidis, M. G. *J. Am. Chem. Soc.* **2002**, *124*, 12255-12260.

(4) Trikalitis, P. N.; Rangan, K. K.; Kanatzidis, M. G. *J. Am. Chem. Soc.* **2002**, *124*, 2604-2613; Rangan, K. K.; Trikalitis, P. N.; Canlas, C.; Bakas, T.; Weliky, D. P.; Kanatzidis, M. G. *Nano Lett.* **2002**, *2*, 513-517; Trikalitis, P. N.; Rangan, K. K.; Bakas, T.; Kanatzidis, M. G. *Nature* **2001**, *410*, 671-675.